

# Evidence of a low temperature dynamical transition in concentrated PNIPAM microgels

Marco Zanatta,<sup>1</sup> Letizia Tavagnacco,<sup>2</sup> Elena Buratti,<sup>3</sup> Monica Bertoldo,<sup>3,\*</sup>  
 Francesca Natali,<sup>4</sup> Ester Chiessi,<sup>5</sup> Andrea Orecchini,<sup>6,†</sup> and Emanuela Zaccarelli<sup>2,‡</sup>

<sup>1</sup>*Department of Computer Science, University of Verona, Strada Le Grazie 15, 37138, Verona, Italy*

<sup>2</sup>*CNR-ISC and Department of Physics, Sapienza University of Rome, Piazzale A. Moro 2, 00185, Rome, Italy*

<sup>3</sup>*CNR-IPCF Istituto per i Processi Chimico-Fisici,*

*Sede Secondaria di Pisa, Consiglio Nazionale delle Ricerche,*

*Area della Ricerca, via G. Moruzzi 1, 56124 Pisa, Italy*

<sup>4</sup>*CNR-IOM, Operative Group in Grenoble (OGG), c/o Institut Laue Langevin,  
 6 rue Jules Horowitz, BP 156, 38042 Grenoble cedex 9, France*

<sup>5</sup>*Department of Chemical Sciences and Technologies,*

*University of Rome Tor Vergata, Via della Ricerca Scientifica 1, 00133 Rome, Italy*

<sup>6</sup>*Department of Physics and Geology, University of Perugia and CNR-IOM, Via A. Pascoli, 06123, Perugia, Italy*

(Dated: December 3, 2024)

By combining elastic incoherent neutron scattering experiments and molecular dynamics simulations, we explore the low temperature behavior of hydrated PNIPAM microgels, a popular model system to study glassy and jammed states. We find that the complex internal architecture of microgel particles is highly efficient in avoiding water crystallization, allowing us to detect a dynamical transition at a temperature around 250 K. The direct comparison between experiments and simulations shows a quantitative agreement, providing evidence that the transition occurs simultaneously for PNIPAM and water dynamics. Our results have strong similarities with the celebrated protein dynamical transition, suggesting its occurrence in different macromolecular systems, independently from their biological function. Our findings could help to shed light on the controversial, still elusive, nature of such phenomenon.

Microgels are colloidal-scale particles[1], widely used in several applications, spanning from drug delivery to sensing[2, 3]. The most studied microgels are based on poly-N-isopropyl-acrylamide (PNIPAM), a thermoresponsive polymer that is soluble in water at room temperature but becomes insoluble on heating. The well-established synthesis protocol[4] yields microgel particles dispersed in water with diameters ranging from about 50 nm to a few microns. These colloids, internally made by heterogeneously crosslinked PNIPAM networks, undergo a reversible Volume Phase Transition (VPT) from a swollen state at temperatures  $T$  below the  $T_{VPT} \sim 305$  K to a collapsed state at higher temperatures[1].

PNIPAM microgels are nowadays mostly studied at temperatures across the VPT temperature, being exploited as a tunable model system for elucidating phase transitions and glassy behavior[5]. The dual colloidal/polymeric nature of microgels[6] bridges the properties of classical hard-sphere colloids and soft polymeric particles[7], opening up the possibility of investigating two distinct glass transitions. In the swollen regime, for  $T \lesssim T_{VPT}$ , a colloidal glass transition takes place at an effective (colloidal) volume fraction of about 0.6[8], which amounts to only  $\sim 10\%$  in PNIPAM weight fraction (wt)[9]. Such dilute conditions leave ample margin for residual mobility of the internal (polymeric) degrees of

freedom. On the other hand, it has been reported that in the same temperature window linear PNIPAM chains in water undergo a polymeric glass transition around 80%wt [10, 11]. The intermediate concentration region in between the colloidal and polymeric glass transitions (10%-80%wt) has rarely been investigated so far for PNIPAM microgels. Indeed, the non-ergodic nature of the samples on large length and time scales poses challenges to experimental investigations in terms of sample reproducibility and stability over time. Furthermore, the investigation of very concentrated microgels opens up the possibility to explore their behavior at low temperatures avoiding water crystallization. Indeed, for PNIPAM chains, crystallization was shown to be absent for polymer weight fractions above  $\sim 50\%$  [10, 11].

In this work we tackle an unprecedented region of PNIPAM microgels phase diagram, encompassing weight fractions in the range  $40 \leq c \leq 95\%$ wt and a wide range of temperatures below  $T_{VPT}$ , i.e.  $150 \lesssim T \lesssim 293$  K. By combining elastic incoherent neutron scattering experiments (EINS) and all-atom molecular dynamics (MD) simulations, we probe the internal dynamics of microgels at short time and length scales. We find that our suspensions do not crystallize for PNIPAM mass fractions  $\gtrsim 43\%$  at any temperature and, most importantly, that the system undergoes a clear “dynamical” transition at  $T_d \approx 250$  K, akin to that observed in proteins. Thanks to a robust and reliable preparation protocol, our measurements are fully reproducible, showing a smooth dependence on PNIPAM mass fraction. We directly compare the measured EINS intensities and their associated mean-

\* monica.bertoldo@pi.ipcf.cnr.it

† andrea.orecchini@unipg.it

‡ emanuela.zaccarelli@cnr.it

squared displacements (MSD) with those calculated in simulations, finding quantitative agreement between the two. Moreover, simulations show a clear signature of the dynamical transition for both PNIPAM and water dynamics.

The dynamical transition has been reported in a number of different proteins and other bio-macromolecules in water [12–14]. It occurs in the supercooled region at a temperature that is usually higher than the glass transition temperature[15]. The dynamical transition is associated to a sudden increase with temperature of the protein atom MSD, due to the onset of anharmonic degrees of freedom and accompanied by the activation of biological functionality. Indeed, anharmonic motions allow the protein to explore those conformational substates corresponding to the structural configurations of functional relevance.

Notwithstanding the large amount of activity on this topic, the microscopic origin of the protein dynamical transition remains nowadays widely debated, particularly for what concerns the role played by water[16, 17]. Building on the similarity between proteins and PNIPAM, already established 20 years ago[18], the evidence provided in this work could help to shed light on this controversial aspect. In addition, our results suggest a generality for the concept of a low temperature dynamical transition in disordered macromolecules with internal degrees of freedom. We expect that these findings will stimulate further work on this subject and will have significant impact in the context of hydrated suspensions with both biological and non-biological implications.

## RESULTS

### EINS experiments

EINS experiments were performed on hydrogenated PNIPAM microgels in D<sub>2</sub>O at several PNIPAM mass fractions, from 43% to 95% [19]. In thermal neutron scattering, the incoherent cross-section of hydrogen atoms is more than an order of magnitude larger than both coherent and incoherent cross-sections of the other atomic species present in our PNIPAM mixtures. Therefore, the incoherent signal of the hydrogenated PNIPAM network dominates the mostly coherent signal of deuterated water, providing selective access to the microscopic dynamics of the polymer matrix.

Data were collected at the backscattering spectrometer IN13 of the Institut Laue-Langevin (ILL, Grenoble, France). This instrument has an energy-resolution  $\Delta E = 8 \mu\text{eV}$  (FWHM) and covers a momentum transfer interval from 0.3 to 4.5  $\text{\AA}^{-1}$ , thus making accessible motions faster than about 150 ps occurring in the spatial region between 1 and 20  $\text{\AA}$ . In this way, we essentially probe the internal dynamics of the microgels and its behavior on the atomic scale. This is important because, even though these samples are glassy on the colloidal

scale [8, 9], the volume fraction occupied by the microgels is still much lower than that of the polymer glass transition, so that we can safely assume that the polymeric degrees of freedom are in equilibrium. Indeed our results confirm this assumption, as they do show a progressive and smooth behavior with PNIPAM mass fraction, are reproducible with respect to sample preparation and are fully reversible in temperature.

The measured incoherent elastic intensities  $I(Q, 0)$  as a function of temperature and momentum transfer  $Q$  are reported in Fig.1(a) for selected samples with PNIPAM mass fraction (wt) of 43% and 60%. Data were recorded under thermal cycles of cooling (upper panels) and heating (lower panels) in a range of temperatures between 287 K and 152 K. The temperature behaviour is best observed in the  $Q$ -integral of  $I(Q, 0)$ , reported in Fig. 1(b). Upon cooling, the integrated elastic intensity progressively increases until a sharp variation occurs at a characteristic “dynamical transition” temperature  $T_d \sim 250$  K, below which the intensity increase continues with a smaller but linear slope. Such a discontinuity is more pronounced at the lowest PNIPAM concentration and gradually disappears with decreasing water content. Upon heating back, the measured data fall on top of the corresponding ones at the same  $T$ , confirming the full reversibility of the process.

At each temperature, the average atomic mean squared displacements (MSD) can be calculated from the  $Q$ -dependence of  $I(Q, 0)$  (see SI). The resulting MSD in Fig. 1(c) reflect the discontinuity at  $T_d \sim 250$  K. The linear temperature evolution of the MSD below  $T_d$  is typical of a harmonic solid. The sudden slope increase above  $T_d$  witnesses an enhanced mobility of the PNIPAM atoms, due to the onset of anharmonic motions and resulting in the corresponding elastic intensity drop.

The observed slope discontinuity at  $T_d$  might be attributed to an underlying crystallization process associated to the D<sub>2</sub>O. However, the measured  $I(Q, 0)$  for pure D<sub>2</sub>O in the same temperature range shows defined crystalline peaks that do not appear in low- $T$  PNIPAM suspensions (see SI, Fig. S3). This suggests that the elastic intensity drop of the PNIPAM network originates from a mechanism other than water crystallization.

### MD Simulations

To identify the microscopic mechanism which is responsible for the observed change in PNIPAM dynamics taking place at  $T_d$ , we rely on all-atom MD simulations. To this aim, we have designed a new microgel model (described in Materials and Methods and SI) and performed its numerical investigation at mass fractions of 40% and 60%. A snapshot of the *in silico* microgel model is displayed in Fig.2(a). The PNIPAM network has been built with a crosslinker/monomer ratio of 1/28 which, taking into account the inhomogeneous density of a PNIPAM particle, describes an inner region (e.g. the core region)

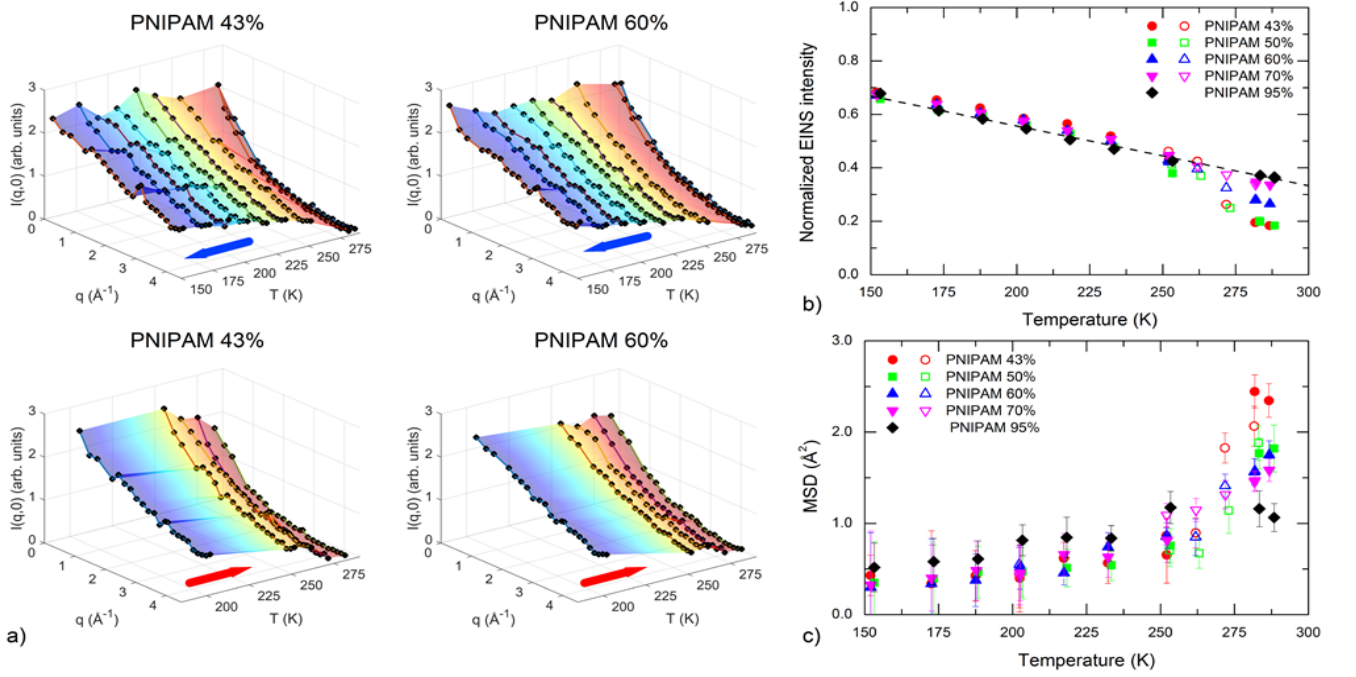


FIG. 1. EINS data. a) Incoherent elastic intensities  $I(Q, 0)$  measured on PNIPAM microgels in  $D_2O$  with a mass fraction concentration of 43% and 60% as a function of temperature  $T$ . Top (bottom) panels reports data recorded under cooling (heating). b) Integral over  $q$  of  $I(Q, 0)$  as a function of  $T$ ; measurements under cooling are presented with filled symbols whereas those under heating with open symbols. c) Temperature evolution of MSD as obtained using the double well model (see SI).

of the microgel. The number of water molecules per monomeric unit is smaller than the experimentally determined value of hydration molecules for PNIPAM microgels [20] for both concentrations. Thus, we can safely assume that all water molecules in the simulations are hydration water and not bulk water.

At each studied temperature, we monitor the dynamics of both microgel and water atoms separately. To characterize microgel dynamics we start by calculating the self intermediate scattering (SISF) function which probes the single-particle translational dynamics at a characteristic wavevector. Fig. 2(b) displays the SISFs calculated for the 40% mass fraction case for PNIPAM hydrogen atoms at a transferred wave-vector of  $Q = 2.25 \text{ \AA}^{-1}$ , that corresponds to the first peak of the oxygen-oxygen structure factor of bulk water [21]. PNIPAM internal dynamics exhibits a two-step behavior typical of glass-forming liquids: an initial fast relaxation is followed by a long-time, slow relaxation indicating structural rearrangement. At the lowest studied temperatures, the SISFs do not decay completely to zero, an indication that the system is becoming arrested on the considered time window. Longer timescale have been considered, revealing that aging phenomena do not play a major role at the studied temperatures (see SI, Figs. S5 and S6). The long-time relaxation of the SISFs is well described by a stretched exponential as in standard glass-formers, thus providing an estimate of the structural relaxation time  $\tau_p$ . This is shown

in Fig. 3(a) as a function of temperature in an Arrhenius plot. We find that  $\tau_p$  obeys two distinct dynamical regimes, each characterized by Arrhenius dependence. The crossover temperature of about 250 K is strikingly similar to that found in EINS experiments. The activation energies are  $\sim 28.4 \text{ kJ mol}^{-1}$  and  $\sim 14.5 \text{ kJ mol}^{-1}$  for the high and low temperature regime, respectively.

To complement these results, we also investigate the hydration water dynamics by looking at the mean-squared displacements (MSD) of the oxygen atoms, which are reported in Fig. 2(c). Similarly to the PNIPAM SISFs, we observe a slowing down of water dynamics with decreasing  $T$ . While at high  $T$ , the MSD shows a diffusive behavior in the studied time interval, upon lowering temperature the onset of an intermediate plateau is observed. This is a characteristic feature of glassy systems, indicating that atoms remain trapped in cages of nearest neighbours for a transient, before eventually diffusing away at long times. Water oxygen atoms retain a diffusive behavior at all studied  $T$ , so that it is possible to estimate their self-diffusion coefficient  $D_w$ . This is also reported in the Arrhenius plot of Fig. 3(a), where  $D_w$  is also found to follow two distinct Arrhenius regimes, crossing again at a temperature  $\approx 250 \text{ K}$ . Furthermore, in the inset of Fig. 2(c) the water MSD calculated at a time of 150 ps, matching the experimental time resolution, is reported as a function of  $T$ . A clear increase of the MSD above  $\sim 250 \text{ K}$  is found, a behavior that

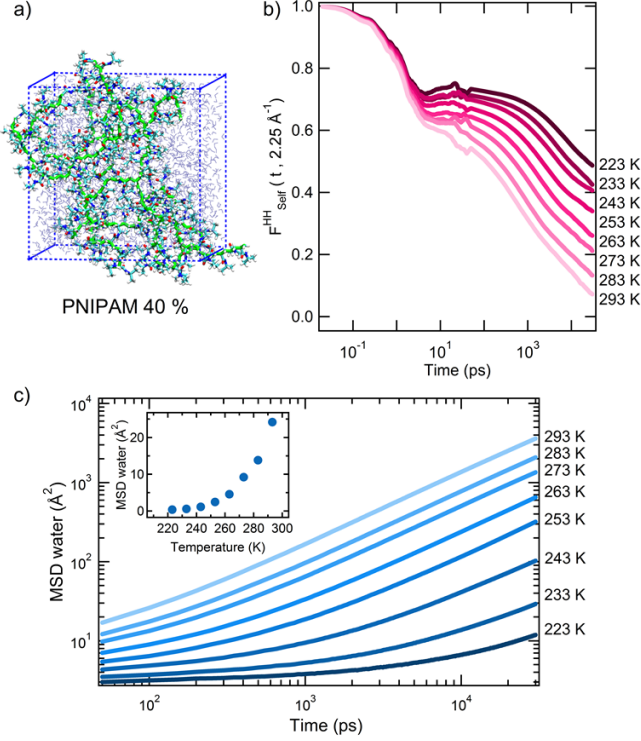


FIG. 2. MD simulations results for 40% mass fraction. a) Snapshot of the simulation of PNIPAM microgel showing a typical configuration of the system. Chain atoms are displayed in green to highlight the microgel structure. b) Self-intermediate scattering function of the PNIPAM hydrogen atoms calculated at  $Q = 2.25 \text{ \AA}^{-1}$  as a function of temperature. c) Time-evolution of the mean square displacements of water molecules from the simulation of the PNIPAM microgel. The inset shows the water mean square displacements values at 150 ps as a function of  $T$ .

is strikingly reminiscent of that observed in experiments and simulations of hydrated proteins[16, 17].

To make a closer connection to protein dynamics, we also calculate the root mean square fluctuation (RMSF) of PNIPAM hydrogen atoms, which measures the fluctuations of the atom positions with respect to the averaged structure over a defined period of time. We monitor this quantity separately for hydrogen atoms of the methyl groups and those of the backbone. The evolution with temperature of the RMSF for both types of hydrogen atoms, averaged over the experimental resolution time, is shown in Fig. 3(b). Again, a clear change is detected at a temperature  $\sim 250 \text{ K}$  for both types of atoms with a stronger effect for the backbone hydrogen atoms. Such a change is observed for both studied mass fractions, suggesting that concentration does not play any role on the value of the crossover temperature, for both water and PNIPAM atoms, but it only smears out the variation, making the two regimes progressively similar to each other. These findings are in agreement with the concentration dependence of  $I(Q, 0)$  (Fig. 1b).

Fig. 3(a) summarizes the MD results, comparing the

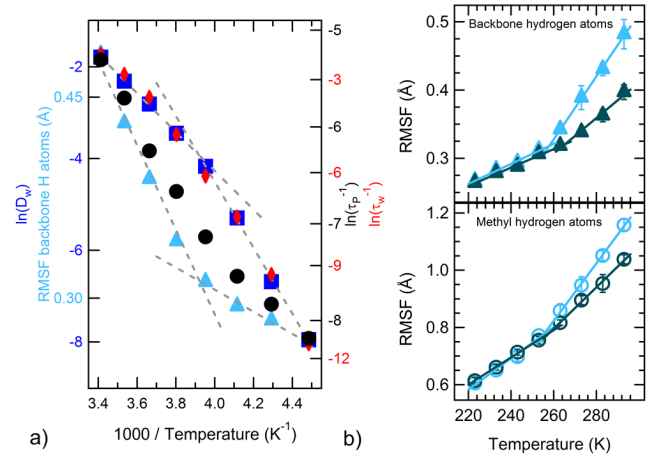


FIG. 3. Water-PNIPAM coupling. a) Temperature dependence of water diffusion coefficient (squares); SISF relaxation times for PNIPAM hydrogen atoms (circles) and water oxygen atoms (diamonds) and root mean square fluctuation (RMSF) of backbone hydrogen atoms (triangles) calculated from MD simulations. Dashed lines are guides to the eye. b) Temperature evolution of RMSF of the PNIPAM hydrogen atoms for 40% wt (light blue) and for 60% wt (dark green) averaged over 150ps: methyl groups (circles), backbone atoms (triangles).

behavior of  $\tau_p$  and RMSF of PNIPAM backbone atoms as well as the self-diffusion constant of water and the associated relaxation time  $\tau_w$ . All these quantities show a clear change of behavior at a temperature  $\sim 250 \text{ K}$ , which is roughly the same as the one for which the EINS data reveal a variation. The simulations clearly indicate that this change occurs simultaneously both for PNIPAM and for water dynamical properties, which are then slaved to each other. These results suggest to interpret the temperature at which the variation in the dynamics occurs as the analogue of the protein dynamical transition for PNIPAM microgels suspensions. Thus, we claim that PNIPAM microgels show a dynamical transition at  $T_d \sim 250 \text{ K}$ . Indeed, several features are shared by the two phenomena. First of all, the strong coupling between water and PNIPAM dynamics, reported in Fig. 3(a), has also been established by a series of studies for hydrated proteins [22, 23] and recently confirmed even for intrinsically disordered proteins [24]. The latter study has further shown that the same protein studied in dry conditions would not exhibit the dynamical transition. Similarly, dry PNIPAM microgels at 95%wt do not show a variation in the dynamics. Finally, in both cases it is found that the dynamical transition takes place at a temperature that is higher than the glass transition one.

It is then natural to ask whether water drives the occurrence of such dynamical transition, being ubiquitous in proteins, either folded or intrinsically disordered, and in PNIPAM microgels suspensions. To partially answer this question, we refer to recent simulation studies on confined water, that have provided a detailed characterization of the water slow dynamics [25]. In particu-

lar the study of hydrated lysozyme [26] has identified a new (long) timescale governing the behavior of confined water, which is characterized by two distinct Arrhenius regimes, in full analogy with the present findings for water confined in microgels. Such a behavior was interpreted as a strong-strong transition due to the coupling of hydration water with the fluctuations of the protein structure and was found to occur in correspondence of the protein dynamical transition.

In our simulations, we find the same phenomenology, suggesting that indeed hydration water drives the occurrence of the dynamical transition. In support of this idea comes the fact that the behavior with concentration is similar for both PNIPAM microgels and hydrated proteins. The less water in the system, the weaker is the dynamical variation, until it disappears for dry samples [24, 27]. Further work is needed to clarify this point, because it remains a controversial one. Indeed, very recent work has reported opposite results suggesting that even dry proteins may have a dynamical transition [28], possibly being it related to the intrinsic disorder of the protein energy landscape, a feature that is however shared by PNIPAM microgel networks.

### Comparison between MD simulations and EINS data

We now turn to provide a direct comparison between experimental and numerical data. In order to do so, we have calculated the elastic intensity in simulations, as explained in Supporting Information. The resulting  $I(Q, 0)$  as a function of  $Q$  are reported in Fig. 4 for simulations (a) and experiments (b) at corresponding temperatures for 40%wt. The data are in very good qualitative agreement, also showing the presence of more pronounced peaks at comparable wavevectors. Both sets of data were fitted with a double-well model (see SI, Fig. S1 and S2). The model captures the data behavior very well, even if it is strictly valid only for the incoherent part of  $I(Q, 0)$ . This confirms that the incoherent contribution is largely dominant in our measurements. To visualize this, we report the comparison of total and incoherent  $I(Q, 0)$  in simulations with their relative fits in SI, Fig. S7. The fit to a double-well model provides the experimental mean-squared displacements of the system, which are reported in Fig. 4(c) for both 43% and 60% PNIPAM mass fractions. They are found to be superimposed to the numerical results of the fits (see SI) without any scaling of the data. However, from the simulations we can calculate the MSD of all types of atoms, being able directly compare with the results of the fits of experimental  $I(Q, 0)$ . We thus plot the MSD of PNIPAM hydrogen atoms in Fig. 4(c), finding that it quantitatively agrees with the experimental estimates for both studied PNIPAM mass fractions. This indirectly confirms that our experiments correctly probe only the incoherent contribution from PNIPAM hydrogen atoms.

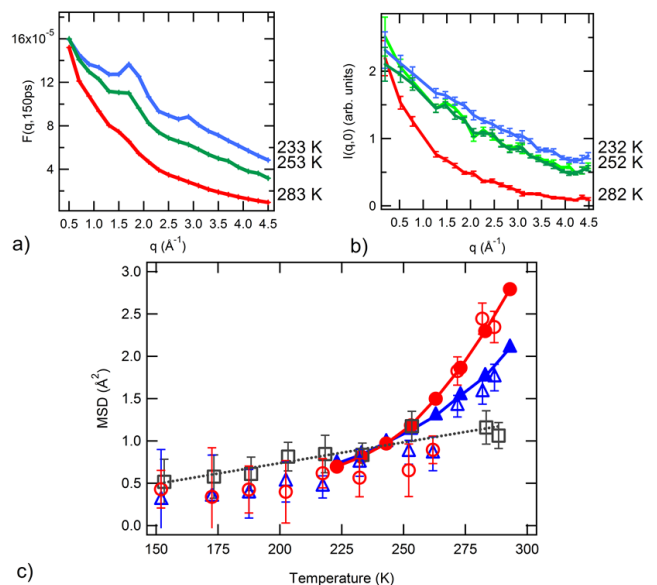


FIG. 4. Quantitative comparison between experiments and simulations. a) Neutron spectra as a function of temperature as calculated from the MD simulations of the PNIPAM microgel at 40%. The total intermediate scattering functions are displayed at a value of 150 ps for comparison with the experimental data. b) EINS spectra measured on the sample with a PNIPAM concentration of 43% as a function of temperature. Data shown at 252 K compare the spectra measured under cooling of the sample (dark green) and under heating of the sample (green). c) Temperature dependence of experimental (open symbols) MSD for PNIPAM mass fractions 43% (circles), 60% (squares) and 95% (triangles) and numerical (filled symbols) MSD, calculated at 150 ps for PNIPAM hydrogen atoms only, for PNIPAM mass fractions 40% (circles) and 60% (squares). The dashed line is a guide to the eye suggesting a linear behavior for the dry sample, for which the dynamical transition is suppressed.

### DISCUSSION AND CONCLUSIONS

In this work we have reported evidence of the occurrence of a dynamical transition in concentrated PNIPAM microgels suspensions at low temperatures, akin to that observed in proteins. We have combined elastic incoherent neutron scattering measurements with atomistic MD simulations, based on a new model specifically developed to mimic the interior of a microgel network. While a detailed numerical representation of a whole microgel is currently unfeasible, our study is capable to resolve the intra-network dynamics of PNIPAM atoms at the short timescales probed by EINS experiments. At the studied concentrations, the microgel samples are macroscopically arrested in a glass-like state, but significant motion is still present for the fast degrees of freedom of the network. Our study considerably extends the range of explored concentrations usually investigated in microgel studies and shows that we can gain novel physical understanding by focusing on very concentrated sam-



ples, up to the polymeric glass transition. A legitimate question concerns the reproducibility and the stability of our samples at these high concentrations. In particular, one could ask whether a homogeneous sample can be obtained, with water uniformly distributed in all the available volume. A careful preparation and measurement protocol allowing to obtain and investigate homogeneous samples, described in Materials and Methods, has been applied, which has ensured complete reproducibility of the results and a smooth, progressive variation with microgel concentration. These results open up the possibility to systematically investigate very high concentration samples, beyond current practice.

The study of microgels in water at low temperatures poses the numerical challenge to appropriately identify a suitable water model, able to realistically describe its peculiar behavior. Very accurate models exist which are usually able to describe specific aspects, in particular TIP4P/ICE was devised to accurately reproduce the solid properties of water [29]. We have chosen to work with such a model because it was found to predict water melting at  $\sim 270$  K, as compared to the most widely adopted TIP4P/2005 [30] which predicts it at  $\approx 250$  K. Thus, it is expected to be more realistic also in describing supercooled water environments. Indeed, our results have confirmed this hypothesis providing quantitative agreement with experiments in all the investigated  $T$ -range for the dynamical properties of PNIPAM atoms. It will be interesting to test other models, particularly TIP4P/2005, under the same conditions as well as to extend our studies at higher temperatures, around the VPT of PNIPAM microgels.

We have demonstrated the ability of high PNIPAM concentration samples to avoid water crystallization, making it possible to investigate PNIPAM microgels at unprecedentedly low temperatures. Indeed, since all water molecules are effectively confined within the network structure, the system remains disordered in the whole investigated  $T$ -range, showing the onset of a dynamical transition in the supercooled regime. This transition shares many features with those commonly observed in proteins and could help to shed light on its controversial nature. Our results show that the transition occurs simultaneously for both PNIPAM and water dynamics, making it plausible that water plays a driving role in this phenomenon. It appears that microgels are extremely efficient in confining water, because the lower limit of sample crystallization is close to 40% PNIPAM mass fraction, a value that exceeds in amount of water what commonly found in other confining environments. Indeed, the typical protein concentration where crystallization is avoided is  $\approx 60\%$  in protein mass fraction [12–14, 24]. Thus, our study suggests that stable samples with a majority of water can be studied down to very low temperatures, which could be of potential interest for the investigation of liquid-like water behavior in the so-called no man's land region of the phase diagram. The efficient confinement role played by microgels is probably due to their

intrinsic network disorder and to their inhomogeneous internal architecture. However, it would be interesting to investigate other macromolecular environments with similar properties that could also be appropriate for suppressing water crystallization. It would then be natural to expect that these systems would also display a dynamical transition, similar to that observed here, that could be considered as a general feature of water hydrating complex macromolecular suspensions.

## MATERIALS AND METHODS

### Sample preparation

Microgels have been synthesized by precipitation polymerization at  $T = 343$  K of N-isopropylacrylamide (NI-PAM) in water (0.136 M) in the presence of N,N'-methylenebisacrylamide (BIS) (1.82 mM). The reaction was carried out in presence of 7.80 mM sodium dodecyl-sulfate as surfactant and potassium persulfate (2.44 mM) as radical initiator. The reaction was carried out for 10 h in nitrogen atmosphere. The obtained colloidal dispersion was purified by exhaustive dialysis against pure water, lyophilized, dispersed in D<sub>2</sub>O, lyophilized and dispersed again in D<sub>2</sub>O to a final concentration of 10%. The obtained microgels have been characterized by dynamic light scattering (Zetasizer Nano S, Malvern) and the hydrodynamic diameter was found to be  $94.0(\pm 3.2)$  nm at 293 K with a size polydispersity of  $0.17(\pm 0.01)$ .

### EINS experiments

EINS experiments were carried out on PNIPAM microgel suspensions with a PNIPAM mass fraction of 43%, 50%, 60%, 70%, and 95% (dry sample). To single out the incoherent signal from PNIPAM hydrogen atoms samples were prepared in D<sub>2</sub>O. Measurements were performed at the backscattering spectrometer IN13 of the Institut Laue-Langevin (ILL, Grenoble, France). PNIPAM samples were measured inside flat aluminum cells ( $3.0 \times 4.30$  cm), sealed with an In o-ring. The thickness of the cell was adjusted to achieve a transmission of about 88% for each sample. Samples at the required concentrations were obtained by filling sample holders with PNIPAM dispersion at 10% and by allowing the exceeding D<sub>2</sub>O evaporating at room temperature under vacuum. Once the desired concentration was reached, holders were sealed and samples were left to homogenize for not less than four days. EINS data were acquired in the fixed-window elastic mode, thus collecting the intensity elastically scattered as a function of the wavevector transfer  $Q$ . Data were corrected to take into account incident flux, cell scattering, and self-shielding. The intensity of each sample was normalized with respect to a vanadium standard to account for the detector efficiency. Multiple scattering processes have been neglected. The

measured elastic intensity has been interpreted by exploiting the double-well model (see SI).

### PNIPAM model and MD Simulations

The model used in the MD simulations mimics, with an atomic detail, a cubic portion of the PNIPAM microgel having a box size of about 4.3 to 3.7 nm, for a polymer concentration of 40 and 60%wt, respectively. The macromolecular network, modelled as isotropic, includes 12 atactic PNIPAM chains jointed by 6 4-fold bisacrylamide cross-links (see Figure S4). Amide groups of PNIPAM residues are represented in the trans conformation. The 3-D percolation of the polymer scaffold is accounted by the covalent connectivity between adjacent periodic images. The number average molecular weight of chains between cross-links,  $M_c$ , is 1584 g/mol, with a polydispersity index of 1.02. Such  $M_c$  value corresponds to an average degree of polymerization of 14. A number of water molecules in agreement with the experimental average degree of hydration is included. Taking into account the NIPAM/BIS feed ratio used in the synthesis and the not uniform cross-links density of PNIPAM microgels, this model can be considered as representing a region in proximity to the core-shell boundary of the microparticle. Atomistic molecular dynamics simulations of PNIPAM microgels were carried out at 8 temperatures (293 K, 283 K, 273 K, 263 K, 253 K, 243 K, 233 K, and 223 K). A total trajectory interval of about 0.5  $\mu$ s was calculated for each polymer concentration. Additional details on the simulations are given in the SI Text.

### ACKNOWLEDGMENTS

MZ, LT and EB equally contributed to this work. LT, MB, EC and EZ acknowledge support from European Research Council (ERC-CoG-2015, Grant No. 681597 MIMIC). MB, AO and EZ acknowledge support from MIUR-PRIN. We acknowledge ILL for beamtime.

## SUPPORTING INFORMATION

### Preparation and stability of the samples for EINS measurements

To obtain samples with the required PNIPAM concentration within the cell employed at IN13, we started from the prepared microgel dispersion at 10%. We then proceeded by evaporation of the exceeding D<sub>2</sub>O in dry atmosphere, using a desiccator under moderate vacuum ( $\sim 10$  mmHg). Once reached the final concentration, cells were sealed and left to homogenize at room temperature for at least four days before analysis. The sample at 95% composition was prepared from film casting the PNIPAM dispersion at 10% up to dryness in Petri dish. The obtained transparent films were milled with an IKA MF 10.1. Cutting-grinding give rise to a rough powder that was poured into an aluminum cell for neutron scattering. It is important to note that, after EINS measurements were performed, cells were opened and no changes in the samples morphology were detected, showing a homogeneous character and no compartmentalization effects.

### EINS measurement and data analysis

In the incoherent approximation, the elastic neutron scattering intensity  $I(Q, 0)$  can be described by the double-well model [12]. Within this approximation, hydrogen atoms are supposed to be dynamically equivalent and may jump between two distinct sites of different free energy. The elastic intensity can be thus written as

$$I(Q, 0) = \exp(-Q^2 \langle \Delta u^2 \rangle_{vib}) \left[ 1 - 2p_1 p_2 \left( 1 - \frac{\sin(Qd)}{Qd} \right) \right] \quad (1)$$

where  $p_1$  and  $p_2$  are the probabilities of finding the hydrogen atom, respectively, in the ground and excited state,  $\langle \Delta u^2 \rangle_{vib}$  corresponds to the vibrational mean square displacement of protons rattling in the bottom of the wells, and  $d$  is the distance between the two wells. In this model, where a transition between the two states represents a jump between conformational substates in the free energy surface, the amplitude of the 3-dimensional structural fluctuations is given by the relationship [31]:

$$\langle \Delta r^2 \rangle = -6 \left( \frac{d \ln I(Q)}{dQ^2} \right)_{Q=0} = 6 \langle \Delta x^2 \rangle_{vib} + 2p_1 p_2 d^2 \quad (2)$$

Typical examples of the fits to the data with Eq. 1 are shown in Figs. S1 and S2 respectively for 43% and 60% samples. A pure D<sub>2</sub>O sample was also measured to completely rule out the possibility of its crystallization in PNIPAM samples. Fig. S3 shows the  $I(Q, 0)$  for heavy water and for PNIPAM 43% and 60% at 153 K. PNIPAM samples do not show any traces of the D<sub>2</sub>O Bragg peaks.

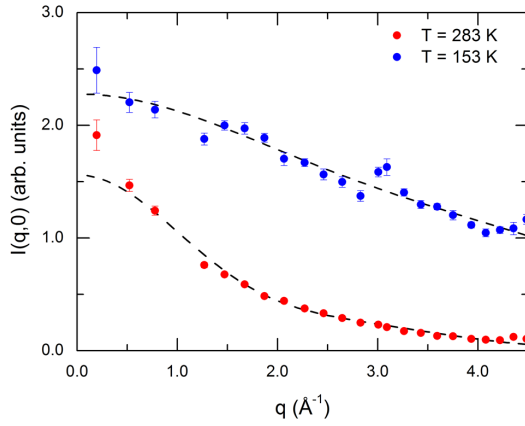


FIG. S1.  $I(Q,0)$  measured on the PNIPAM 43% sample at 283 K (red dots) and 153 K (blue dots); the black dashed line is the fit using Eq. 1.

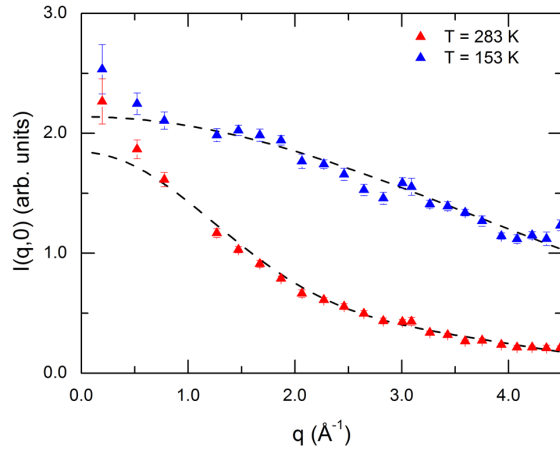


FIG. S2.  $I(Q,0)$  measured on the PNIPAM 60% sample at 283 K (red dots) and 153 K (blue dots); the black dashed line is the fit using Eq. 1.

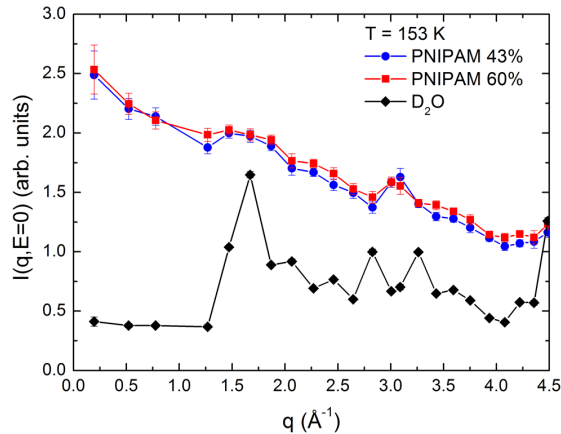


FIG. S3.  $I(Q,0)$  measured on pure  $D_2O$  compared with that obtained on PNIPAM 43% and 60% at 153 K.

## PNIPAM model development

An isotropic polymer scaffold, with the network topology shown in Fig. S4, was built by cross-linking atactic PNIPAM chains in the minimum energy conformation[32]. Amide groups of PNIPAM residues are modeled in the trans conformation. Extra-boundaries covalent connectivity between polymer chains was applied. The network model includes 6 4-fold bisacrylamide junctions and has a number average molecular weight of chains between cross-links,  $M_c$ , of 1584 g/mol, with a polydispersity index of 1.02. The average degree of polymerization of chains between junctions is  $14 \pm 2$ . The polymer scaffold was hydrated by a shell of water molecules to set the PNIPAM concentration in the microgel. Then the system was equilibrated at 293 K in a pressure bath at 1 bar up to a constant density value, i.e. tot-drift less than  $2 \times 10^{-3} \text{ g cm}^{-3}$  over 20 ns. A similar equilibration procedure was applied at each temperature before the NVT run.

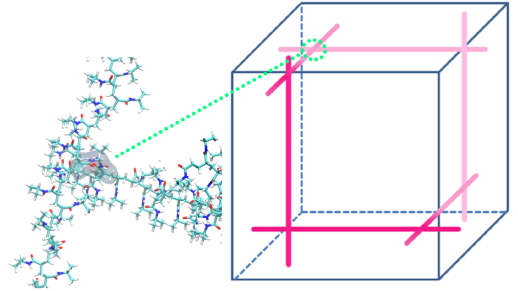


FIG. S4. Schematic representation of the microgel network model.

## MD simulations procedure

Molecular dynamics simulations of PNIPAM microgels were carried out using the GROMACS 5.0.4 software[33, 34]. The polymer network was modeled using the OPLS-AA force field [35] with the implementation by Siu et al. [36], while water was described with the Tip4p/ICE model[29]. The system was equilibrated for 120 ns for  $T \geq 273 \text{ K}$  and for 320 ns for  $T \leq 263 \text{ K}$  in the NPT ensemble, taking into account the longer equilibration time needed at lower temperatures. Simulation data were collected for 330 ns in the NVT ensemble, with a sampling of 0.2 frame/ps. The leapfrog integration algorithm was employed with a time step of 0.2 fs, cubic periodic boundary conditions, and minimum image convention. The length of bonds involving hydrogen atoms was kept fixed with the LINCS algorithm. The temperature was controlled with the velocity rescaling thermostat coupling algorithm with a time constant of 0.1 ps. Electrostatic interactions were treated with the smooth particle-mesh



Ewald method with a cutoff of non-bonded interactions of 1 nm. The last 100 ns of trajectory were considered for analysis. The software MDANSE [37] as well as in-house codes were used for analysis of MD simulations to be compared with the neutron scattering data. Trajectory format manipulations (or conversions) were carried out by the software WORDOM [38]. The software VMD [39] was employed for graphical visualization.

### Reproducibility of numerical results

The numerical data are not affected by aging dynamics on the timescales investigated in the manuscript. To show that this is the case we report the evolution of the MSD upon changing the time interval for the calculation as well as waiting time  $t_w$ . Fig. S5 shows the MSD of water oxygen atoms at the highest ( $T = 293\text{K}$ ) and lowest ( $T = 223\text{ K}$ ) investigated temperatures. We calculate the MSD for a total time of 100 ns and compare it to the corresponding one calculated for only 10 ns (as used in the manuscript, Fig.2(c)). In addition, we also calculate it for  $t_w = 0, 50, 90$  ns. All curves superimpose on the entire investigated timescale, in particular for the intermediate window where the self-diffusion coefficient was extracted, indicated by vertical dashed lines. This behaviour holds for both high and low temperatures. Similarly, Fig. S6 shows the MSD of PNIPAM hydrogen atoms at the same two temperatures over a total interval of 100 and 200 ns, the former being the ones from which we extract the value at 150 ps, reported in the manuscript in Fig. 4c. We also calculate it for waiting times  $t_w = 0, 50, 100\text{ns}$ . At long times, some differences, that are mostly attributable to statistical error rather than aging, are visible. However, it is clear that for the timescale of relevance for comparison with experimental data, i.e. 150 ps, indicated by a vertical dashed line, no significant aging effects are found. This analysis ensures that the numerical data are reproducible and the system is well equilibrated for the short timescales studied in this work.

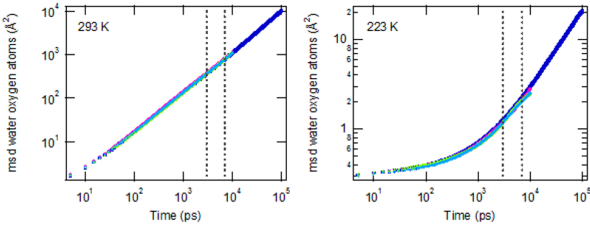


FIG. S5. Comparison between the mean square displacements of water oxygen atoms at 293 K (left panel) and 223 K (right panel) as calculated from the MD simulations over 100 ns of trajectory (blu squares), 0-10 ns (pink diamonds), 50-60 ns (green triangles) and 90-100 ns (light blue circles). Dashed lines highlight the linear region used for water diffusion coefficient calculation.

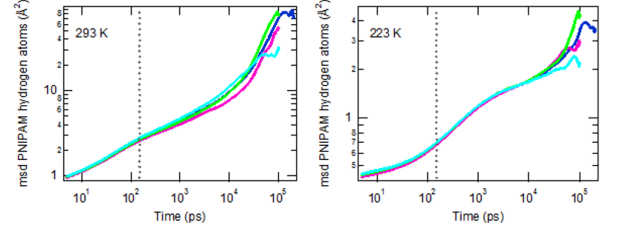


FIG. S6. Comparison between the mean square displacements of PNIPAM hydrogen atoms at 293 K (left panel) and 223 K (right panel) as calculated from the MD simulations over 200 ns of trajectory (blu lines), 0-100 ns (pink lines), 50-150 ns (green lines) and 100-200 ns (light blue lines). The value at the experimental time resolution of 150 ps is indicated with a dashed line.

### Calculation of $I(Q, 0)$ from numerical simulations

We have calculated both the coherent and incoherent intermediate scattering functions for all atoms in the simulations for wavevectors in the range  $0.3 \leq Q \leq 4.5 \text{ \AA}^{-1}$ . By summing the two contributions, weighted by the appropriate scattering lengths and by the partial concentrations, we have obtained the full differential cross-section. Its value at the experimental time resolution of 150 ps provides the numerical  $I(Q, 0)$ . We have further checked that this procedure yields identical results as the calculation of the total dynamical structure factor (in frequency space) convoluted with the experimental resolution. An example of this procedure is provided in Fig.S7.

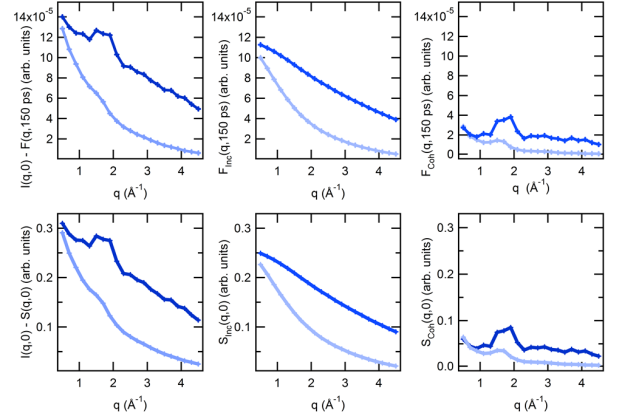


FIG. S7. Comparison between simulated neutron spectra  $I(Q, 0)$  calculated from the intermediate scattering functions at the experimental time resolution of 150 ps (upper panels) and from the total dynamical structure factors convoluted with the experimental resolution (lower panels) at 223 K (blue lines) and 293 K (light blue lines). The incoherent  $F_{Inc}$  and  $S_{Inc}$  are reported in the central panels of each row, while the coherent  $F_{Coh}$  and  $S_{Coh}$  contributions are shown in the rightmost panels.

- 
- [1] A. Fernandez-Nieves, H. Wyss, J. Mattsson, and D.A. Weitz, *Microgel suspensions: fundamentals and applications* (John Wiley & Sons, 2011).
- [2] J.K. Oh, R. Drumright, D.J. Siegwart, and K. Matyjaszewski, *Progress in Polymer Science* **33**, 448 (2008).
- [3] A. Fernández-Barbero, I.J. Suárez, B. Sierra-Martín, A. Fernández-Nieves, F.J. de las Nieves, M. Marquez, J. Rubio-Retama, and E. López-Cabarcos, *Advances in colloid and interface science* **147**, 88 (2009).
- [4] R. Pelton, *Advances in colloid and interface science* **85**, 1 (2000).
- [5] P.J. Yunker, K. Chen, M.D. Gratale, M.A. Lohr, T. Still, and A. Yodh, *Reports on Progress in Physics* **77**, 056601 (2014).
- [6] L.A. Lyon and A. Fernandez-Nieves, *Annual review of physical chemistry* **63**, 25 (2012).
- [7] D. Vlassopoulos and M. Cloitre, *Current Opinion in Colloid & Interface Science* **19**, 561 (2014).
- [8] D. Paloli, P.S. Mohanty, J.J. Crassous, E. Zaccarelli, and P. Schurtenberger, *Soft Matter* **9**, 3000 (2013).
- [9] I. Bischoffberger and V. Trappe, *Scientific reports* **5**, 15520 (2015).
- [10] F. Afroze, E. Nies, and H. Berghmans, *Journal of Molecular Structure* **554**, 55 (2000).
- [11] K. Van Durme, G. Van Assche, and B. Van Mele, *Macromolecules* **37**, 9596 (2004).
- [12] W. Doster, S. Cusack, and W. Petry, *Nature* **337**, 754 (1989).
- [13] J. Smith, K. Kuczera, and M. Karplus, *Proceedings of the National Academy of Sciences* **87**, 1601 (1990).
- [14] K. Wood, A. Frölich, A. Paciaroni, M. Moulin, M. Härtlein, G. Zaccai, D.J. Tobias, and M. Weik, *Journal of the American Chemical Society* **130**, 4586 (2008).
- [15] S. Capaccioli, K. Ngai, S. Ancherbak, and A. Paciaroni, *The Journal of Physical Chemistry B* **116**, 1745 (2012).
- [16] S.H. Chen, L. Liu, E. Fratini, P. Baglioni, A. Faraone, and E. Mamontov, *Proceedings of the National Academy of Sciences* **103**, 9012 (2006).
- [17] W. Doster, S. Busch, A.M. Gaspar, M.S. Appavou, J. Wuttke, and H. Scheer, *Physical review letters* **104**, 098101 (2010).
- [18] E.I. Tiktopulo, V.N. Uversky, V.B. Lushchik, S.I. Klenin, V.E. Bychkova, and O.B. Ptitsyn, *Macromolecules* **28**, 7519 (1995).
- [19] E. Zaccarelli, M. Bertoldo, F. Natali, J. Ollivier, A. Orecchini, A. Paciaroni, and M. Zanatta, *Fast and slow dynamics in pnipam microgels*, Institut Laue-Langevin (ILL) (2015), doi: 10.5291/ILL-DATA.9-11-1736.
- [20] Y. Ono and T. Shikata, *Journal of the American Chemical Society* **128**, 10030 (2006).
- [21] F. Sciortino, P. Gallo, P. Tartaglia, and S.H. Chen, *Physical Review E* **54**, 6331 (1996).
- [22] H. Frauenfelder, G. Chen, J. Berendzen, P.W. Fenimore, H. Jansson, B.H. McMahon, I.R. Stroe, J. Swenson, and R.D. Young, *Proceedings of the National Academy of Sciences* **106**, 5129 (2009).
- [23] M. Ferrand, A. Dianoux, W. Petry, and G. Zaccai, *Proceedings of the National Academy of Sciences* **90**, 9668 (1993).
- [24] G. Schirò, Y. Fichou, F.X. Gallat, K. Wood, F. Gabel, M. Moulin, M. Härtlein, M. Heyden, J.P. Colletier, A. Orecchini, A. Paciaroni, J. Wuttke, D.J. Tobias, and Martin Weik, *Nature communications* **6**, 6490 (2015).
- [25] P. Gallo, M. Rovere, and S.H. Chen, *The Journal of Physical Chemistry Letters* **1**, 729 (2010).
- [26] G. Camisasca, M. De Marzio, D. Corradini, and P. Gallo, *The Journal of Chemical Physics* **145**, 044503 (2016).
- [27] U. Lehnert, V. Réat, M. Weik, G. Zaccai, and C. Pfister, *Biophysical Journal* **75**, 1945 (1998).
- [28] Z. Liu, J. Huang, M. Tyagi, H. O'Neill, Q. Zhang, E. Mamontov, N. Jain, Y. Wang, J. Zhang, J.C. Smith, et al., *Physical Review Letters* **119**, 048101 (2017).
- [29] J.L.F. Abascal, E. Sanz, R.G. Fernandez, and C. Vega, *The Journal of Chemical Physics* **122**, 234511 (2005).
- [30] J.L.F. Abascal and C. Vega, *The Journal of Chemical Physics* **123**, 234505 (2005).
- [31] A. Paciaroni, S. Cinelli, and G. Onori, *Biophysical Journal* **83**, 1157 (2002).
- [32] P. Flory, J. Mark, and A. Abe, *Journal of the American Chemical Society* **88**, 639 (1966).
- [33] S. Páll, M.J. Abraham, C. Kutzner, B. Hess, and E. Lindahl, *Tackling Exascale Software Challenges in Molecular Dynamics Simulations with GROMACS* (Springer International Publishing, Cham, 2015), pp. 3-27.
- [34] M.J. Abraham, T. Murtola, R. Schulz, S. Páll, J.C. Smith, B. Hess, and E. Lindahl, *SoftwareX* **1-2**, 19-25 (2015).
- [35] W.L. Jorgensen, D.S. Maxwell, and J. Tirado-Rives, *Journal of the American Chemical Society* **118**, 11225 (1996).
- [36] S.W.I. Siu, K. Pluhackova, and R.A. Böckmann, *Journal of Chemical Theory and Computation* **8**, 1459 (2012).
- [37] G. Goret, B. Aoun, and E. Pellegrini, *Journal of Chemical Information and Modeling* **57**, 1 (2017).
- [38] M. Seeber, A. Felling, F. Raimondi, S. Muff, R. Friedman, F. Rao, A. Caffisch, and F. Fanelli, *Journal of Computational Chemistry* **32**, 1183 (2011).
- [39] W. Humphrey, A. Dalke, and K. Schulten, *Journal of Molecular Graphics* **14**, 33 (1996).